IEEE Access
Multidisciplinary | Rapid Review | Open Access Journal

Received July 13, 2020, accepted July 22, 2020, date of publication July 27, 2020, date of current version August 5, 2020.

Digital Object Identifier 10.1109/ACCESS.2020.3011995

A New Short-Term Prediction Method for Estimation of the Evaporation Duct Height

YANBO MAI[1], ZHENG SHENG[1,2], HANQING SHI[1], CHAOLEI LI[3], QIXIANG LIAO[1], AND JUN BAO[4]

[1]College of Meteorology and Oceanography, National University of Defense Technology, Changsha 410000, China
[2]Collaborative Innovation Center on Forecast and Evaluation of Meteorological Disasters, Nanjing University of Information Science and Technology, Nanjing 210000, China
[3]School of Automation, Southeast University, Nanjing 210000, China
[4]China Satellite Maritime Tracking and Control Department, Jiangyin 214431, China

Corresponding author: Zheng Sheng (19994035@sina.com)

This work was supported in part by the National Natural Science Foundation of China under Grant 41875045 and Grant 41775039, and in part by the Research Projects of National University of Defense Technology under Grant ZK19-21.

ABSTRACT Evaporation duct is a kind of chaotic phenomenon over the ocean. In this paper, a new nonlinear prediction algorithm, the Darwinian evolutionary algorithm (DEA), is introduced to obtain the specific nonlinear formula $P(\cdot)$ of the chaotic phenomenon. Based on Darwinian natural selection and survival theory, the method first selects a suitable training set of samples, and then produces an initial population before going through an evolutionary process of selection, reproduction and mutation until the optimal individual is found. Finally, a specific expression for a nonlinear chaotic time series is obtained, which can realize the short-term prediction of evaporation duct height (EDH) quickly and accurately. After that, the DEA, the support vector regression (SVR), and the back propagation (BP) neural network were applied to predict the EDH which were formed over the ocean by using sounding data. After interpolation and smoothing of the original data, we selected the first 250 data as training samples and the last 115 data as test samples to test the effect of the EDA algorithm. The results showed that the root mean squared error (RMSE) for the DEA was about 7% less than that of the SVR and 10% less than that of BP neural network; the mean absolute percent error (MAPE) for the DEA was about 9% less than that of the SVR and 15% less than that of BP neural network. In addition, the DEA obtained, for the first time, a nonlinear expression for EDH, which provides an important reference for future research on the evaporation ducts.

INDEX TERMS Evaporation duct, nonlinear chaotic time series, Darwinian evolutionary algorithm, support vector regression, back propagation neural network, short-term prediction.

I. INTRODUCTION

Evaporation ducts are a type of near surface duct in the marine environment formed by the evaporation of sea water; due to subjecting to turbulence, weather and other meteorological factors, it is a typical chaotic phenomenon. The duct is an abnormal atmospheric structure in the marine atmospheric environment, and can capture and change the propagation route of electromagnetic waves, thus altering the characteristics of electromagnetic wave propagation [1]. Guo *et al.* [2] pointed out that almost all the sea areas of the world may contain evaporation ducts at any specific time, with the ducts having a certain scale and geographical characteristics which are subject to local weather conditions. Evaporation ducts are sensitive to changes in atmospheric humidity, sea air temperature differences and horizontal wind speed. The formation mechanism of the ducts is due to the unbalanced thermal structures existing between the atmosphere and the ocean boundaries, which lead to sea-air interactions and cause the evaporation of water vapor from the sea surface, such that a large amount of water vapor may reside at the sea surface. After this process and through wind action, the water vapor near the sea surface may diffuse upwards to specific heights, forming a gradient structure whereby there is rapid decrease of water vapor content with height above the surface [1]. The evaporation duct height (EDH) is the main parameter that describes the evaporation duct.

The associate editor coordinating the review of this manuscript and approving it for publication was Kathiravan Srinivasan.

In recent years, many researchers have analyzed and predicted the EDH [3]–[10]. At present, the main methods used to obtain the height include physical measurement, model diagnosis [11] and the radar echo retrieval method [12]. The physical measurement is to obtain a vertical profile distribution of the refractive index of the atmosphere via direct measurement of the atmospheric refractive index at different heights with a microwave refractive index meter, and then calculate the EDH according to the basic definition. The model diagnosis method relies on a specific model to diagnose the EDH by inputting meteorological and hydrological parameters such as air temperature, humidity, atmospheric pressure, wind speed and sea surface temperature for the specific sea area. The radar echo retrieval method is based on measurement of the radar sea clutter power signal to reconstruct the structure of the evaporation ducts. Besides, Freitas and Costa used the ray tracing method [13], [14] to model the evaporation duct [15]. Given that evaporation ducts have a great influence on radar navigation and communication systems, it is important to effectively avoid the negative influences of the evaporation ducts on the radar system. This becomes possible if we can predict the EDH in advance. In recent years, advances in computing, machine learning and intelligent algorithms have become important tools for time series prediction, and such applications in meteorology are becoming more frequent [16]–[22]. For example, based on machine learning, Rhee and Im [23] have used long-range climate forecasting and remote sensing data to forecast meteorological droughts for ungauged areas. Hughes *et al.* [24] used machine learning to predict the global distribution of aerosol mixing state metrics. So far, some scholars also use different machine learning algorithms to predict the EDH [25], [26]. Application of such tools in the study of evaporation ducts would allow us to obtain the EDH information in advance, and thus effectively avoid the negative effects of evaporation ducts on electromagnetic wave transmission. However, the parameters in their algorithms are set according to practical experience, which has certain limitations. Thus, it is essential to establish a powerful and automatic new algorithm to predict the EDH.

In this paper, a new nonlinear prediction algorithm, the Darwinian evolutionary algorithm (DEA) is introduced. Based on the Darwinian natural selection and survival theory, the method first selects a suitable set of training samples, then produces an initial population before going through an evolutionary process of selection, reproduction and mutation until the optimal individual is found. Finally, a specific expression for a nonlinear chaotic time series is obtained to realize the short-term prediction of the EDH. After that, the DEA, the support vector regression (SVR) and the back propagation (BP) neural network were applied to the prediction of the EDH over the ocean. Compared with the SVR and BP neural network, the first advantage of DEA algorithm is to improve the prediction accuracy, and the second advantage is to acquire a nonlinear expression for the EDH, which can obtain the EDH in advance and thus counter the negative effects of the ducts on electromagnetic wave propagation.

II. INTRODUCTION TO EVAPORATION DUCTS AND USE OF DATA

A. INTRODUCTION TO EVAPORATION DUCTS

In the radio meteorology, atmospheric refraction refers to the bending characteristics of electromagnetic waves propagating in the atmosphere. The degree of refraction may be measured by the refraction index n, which is defined as the ratio of the propagation speed c (light speed) of the electromagnetic wave in free space to the propagation speed v in the medium of interest [1]:

$$n = \frac{c}{v} \tag{1}$$

The normal values for the refractive index of the atmosphere at the earth's surface typically range from 1.00025-1.0004. Given the relatively small values, it is not convenient to calculate such values for studies in electromagnetic wave propagation. In order to facilitate the calculation and statistics of refractive index, and evaluate the atmospheric refractive index gradient and its impact on electromagnetic wave propagation more easily, a corrected atmospheric refractive index M [1] is used, that is:

$$M = N + 0.157Z = 77.6 \times \frac{p}{T} + 3.73 \times 10^5 \times \frac{e}{T^2} + 0.157 \times Z \tag{2}$$

where M is the corrected atmospheric refractive index and is a dimensionless quantity. For statistical purposes, M is used as the base unit. N is the atmospheric refractive index and is also a dimensionless quantity. P, T, e and Z are the air pressure, temperature, vapor pressure and height from the ground with units of *hpa*, K, *hpa* and *m,* respectively.

According to the variation of M with height, atmospheric ducts can be divided into the following four categories [10]: surface ducts, surface-based duct, elevated ducts, and evaporation ducts. Figure 1 shows the respective trends of the ducts as a function of height.

The evaporation ducts are a type of near surface duct formed by the evaporation of sea water [1]. The duct is a typical abnormal atmospheric structure in the near sea atmospheric environment, which can capture the propagation of electromagnetic waves, thus altering the characteristics of the electromagnetic wave propagation, and hence having great impact on marine radar, navigation and communication systems. If information on evaporation ducts can be acquired in advance, it is possible to effectively avoid the electromagnetic wave losses caused by the evaporation ducts in the atmospheric environment, and thus ensure reliable over-the-horizon data transmission and target detection at sea.

B. METEOROLOGICAL DATA AND PRETREATMENT

The meteorological data used were high resolution meteorological sounding balloon data [27] and the Defense Meteorological Satellite Program (DMSP) inversion data [10] recorded in 2009. The release site of the sounding balloon

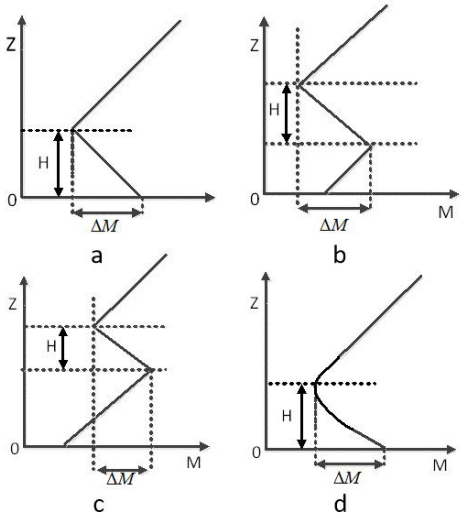

FIGURE 1. (a) Surface ducts (b) surface-based ducts (c) elevated ducts (d) evaporation ducts.

was a sea area near the equator with longitude and latitude of 151.8° E and 7.4° N, respectively; the release time was 12:00 Universal Time Coordinated (UTC) every day. The sounding data recorded meteorological parameters such as temperature, pressure, humidity and wind at the height of the sounding balloon. The vertical resolution below 100 m was 10-80 m, and the vertical resolution above 100 m was 30-300 m. The sea surface temperature (SST) data originated from the DMSP inversion data provided by the National Oceanic and Atmospheric Administration (NOAA) of the USA with a resolution of 0.25°× 0.25°. The longitude and latitude of the selected sites were 151.875° E and 6.375° N, respectively, and the measurement time was 12:00 UTC every day in 2009; the sample size was 365.

First, the temperature, air pressure, relative humidity, wind speed and other meteorological parameters at 3 m height recorded by the sounding balloon were extracted and then substituted into the Liuli-2.0 evaporation duct model [10] to calculate the EDH. Finally, all the diagnostic results were recorded as a time series sample set X. Considering factors such as the rapid change of weather conditions over the sea, measurement errors and turbulence etc., it was necessary to preprocess the data for the EDH before employing the algorithm prediction. First, the abnormal data of the sample set were eliminated. The specific approach adopted was: calculate the mean square deviation σ of the sample data, mark data whose absolute value for the difference between the sample value and the average value is greater than 3σ as "abnormal values", then remove and interpolate the remaining data to get a new data set by cubic spline interpolation [28]; next use the moving average to carry out low-pass filtering to get the a new sample sequence X'. The specific moving average method is as follows [29]:

$$X'_n = \frac{\sum_{i=a}^{n} x_i}{m} \tag{3}$$

where X'_n is the average value of the height of the evaporation duct calculated for the n-th time, x_i is the height of the evaporation duct on the i-th day and a is the first sample in the moving average range. When $n \leq L$, $a = 1$; when $n > L$, $a = n\text{-}L + 1$ (L is the total number of samples); m is the number of samples in the current moving average range. Figure 2 shows the diagnostic results for the EDH and the results after moving average filtering. After moving average filtering, the new time series, X', will be used in the test and analysis of the DEA, the SVR and the BP neural network.

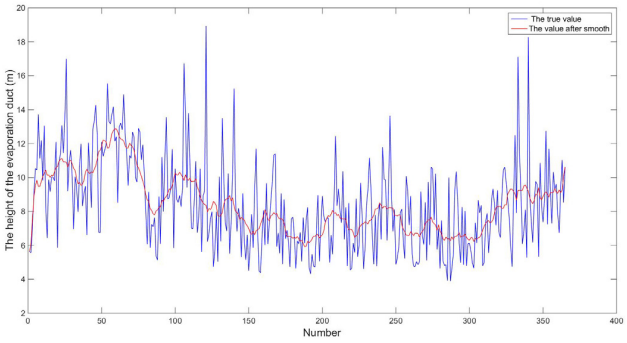

FIGURE 2. The heights of the evaporation ducts obtained after using the Liuli-2.0 model and the heights of the evaporation ducts after smoothing. Abscissa is the sequence of time series, from January 1, 2009 to December 31, 2009, a total of 365 data. The vertical coordinate is the specific value of EDH on that day.

III. THE PREDICTION ALGORITHMS

A. THE SUPPORT VECTOR REGRESSION

The SVR is a classical machine learning algorithm. It breaks through the traditional machine learning methods based on empirical risk minimization theory, where it is easy to produce the over fitting phenomenon for small sample data. It has been widely applied in theoretical research and practical applications and has become a research hotspot in machine learning. The output of SVR is a linear combination of intermediate nodes, each of which corresponds to a support vector. In recent years, it has also been shown to give excellent performance in the prediction of time series and has been successfully applied to the prediction of nonlinear chaotic time series.

In this paper, SVR [30]–[31] is used to analyze and predict the time series X'. The training sample is the first 250 data for the time series X', and the test sample is the last 115 data for the time series X'. The construction of SVM mainly includes the selection of kernel function and parameter. Because the result of solving nonlinear problem by linear kernel function is poor, radial basis function is chosen as kernel function in this paper. The specific formula is as follows.

$$K(x_i, x_j) = \exp\left(-\frac{||x_i - x_j||^2}{2\alpha^2}\right) \tag{4}$$

where x_i and x_j are sample datum and α is hyperparameter. Besides the selection of kernel function, SVR also needs to

set penalty parameter C, insensitivity loss degree ε and kernel function parameter α. The parameter selection is based on grid search method. Firstly, we set a reasonable parameter range according to our experience, then through continuous experiments to test their effect. Finally, the parameters with the best prediction results are selected as the final parameters to predict the EDH. Through test, the final parameter values we finally selected are shown in table 1.

TABLE 1. The specific values parameters of SVR.

Parameter	Specific value
C	10
ε	0.1
α	0.1

B. BP NEURAL NETWORK

Artificial neural network uses mathematical methods to simulate the structure, function, and mode of processing for biological neural systems to build a complete information processing system; so far, it has been widely used in data prediction [32], [33]. In this paper, the BP neural network [34], [35], which is relatively mature and widely used, is used to predict the EDH. The key step of BP neural network is the design of hidden layer. In the BP neural network, the numbers of nodes in input layer and output layer are determined by the training samples, whereas the number of nodes in hidden layer is uncertain. Generally, the number of nodes of the hidden layer can be determined by Eq. (5) [35]:

$$h = \sqrt{m + n + a} \tag{5}$$

where h is the number of nodes of the hidden layer, m is the number of nodes of the input layer, n is the number of nodes of the output layer, and a is the adjustment constant. After comprehensive consideration, we formulate a four-layer BP neural network including an input layer, two hidden layers, and an output layer. The input layer is set to three neurons, the first hidden layer to 5 neurons, the second hidden layer to 2 neurons and the output layer is set to one neuron. Through test, the parameters with the best prediction results are selected as the final parameters to predict the EDH. The final values of h, m, n and a are shown in table 2 and the structure of BP neural network is shown in figure 3.

The excitation function of nodes of the hidden layer of the BP neural network is the rectified linear units (ReLU), a piecewise linear function that which changes all negative values to zero and maintains the positive values.

C. DARWINIAN EVOLUTIONARY ALGORITHM

1) INTRODUCTION TO DARWINIAN EVOLUTIONARY ALGORITHM

The theoretical basis of the DEA is Darwin's natural selection and survival theory. The theory first produces an initial population by selecting the appropriate training set. It then goes

TABLE 2. The specific values parameters of BP neural network.

Parameter	Specific value
h	7
m	3
n	1
a	5

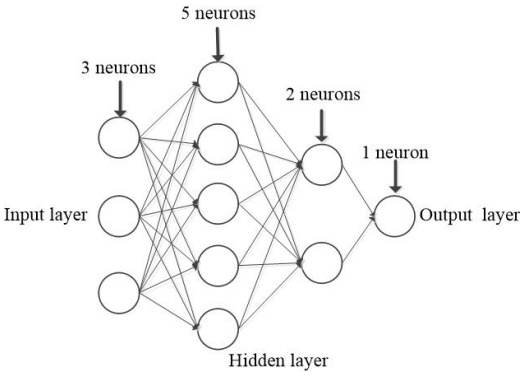

FIGURE 3. The structure of BP neural network.

through the evolutionary process of selection, reproduction and mutation until the optimal individual is found. Finally, the specific expression for the nonlinear chaotic time series is obtained to realize the short-term prediction of the chaotic time series. The basic principle is as follows:

For time series $\{X(t_i)\}, i = 1, \cdots N$, the algorithm can be regarded as the output of a deterministic nonlinear autonomous dynamic system [27]; [29]–[30], which satisfies:

$$\frac{\vec{ds}}{dt} = \phi(\vec{s}) \tag{6}$$

where $\vec{s}$ is a k-dimensional vector and $\phi(\cdot)$ is a nonlinear vector field. Generally, we use a series of observation variables $x(t)$ to describe the system at a certain time, but $x(t)$ is generally complex, which is not conducive to our direct study. To connect the dynamic system (6) with the time series variable $x(t)$, one way to solve this problem is to reconstruct a phase space $h(\cdot)$, that is, $x(t) = \vec{h(s)}$, which is equivalent to its original power system in the topological sense. Through the study of the phase space $h(\cdot)$, we can get the understanding of the original system Φ. However, when dealing with the experimental data, we usually only observe the output of the dynamic system and do not determine the specific state of equation (6). Therefore, we hope to get some useful information about equation (6) from the output of the dynamic system. Takens [39] described the relation between the observation value $x(t)$ at a certain time for the dynamic system and the observation value that preceded it, and this follows the formula:

$$\vec{X}(t) = [x(t), x(t-\tau), \cdots x(t-(m-1)\tau)] \tag{7}$$

When the delay coefficients τ and m are greater than $2de$, (de is the dimension of the attractor, that is, the geometric object generated by the trajectory after the transient disappears), the system will provide a m-dimensional space, which is the replacement of the complete multivariate state space of the system (6). The space in which the attractor exists is a phase space which is a six dimensional imaginary space in which momentum and space occupy three dimensions respectively. Each point above represents all possible states of the system under consideration. The dimension of de can be determined by [40], [41] the embedding dimension m can be determined by [42], and the time delay coefficient τ can be determined by different methods [43], [44]. More specifically, this means that there is a smooth inverse mapping ψ from the k-dimensional state space of the original system to the Euclidean reconstruction space R_m. This mapping is called embedding, and this theorem is called the Takens embedding theorem. The embedding theorem ensures that the state information of the system can be recovered from a long enough output time series observation. According to the theorem, the time series also follows a smooth mapping $P : R^m \to R$:

$$x(t) = P(x(t-\tau), x(t-2\tau), \cdots, x(t-m\tau)) \tag{8}$$

Therefore, the theorem needs two steps to build a dynamic model for the time series. The first step is to reconstruct the current state of the system (state space reconstruction) by using the past state of the time series closest to the current state, which can be achieved by formula (7). The second step is to establish the prediction model $P(\cdot)$ in equation (8). This paper provides a new method to accomplish this step. As long as the state space is reconstructed from the time series, the function $P(\cdot)$ in formula (8) can be estimated.

At present, many researchers have studied the concrete approximate method of $P(\cdot)$ in formula (8). Most of these studies are based on polynomial fitting, neural networks and radial basis functions [36], [37]; [45], [46]. In recent years, a search process based on Darwin's natural selection and survival theory has been proposed [47]–[50]. The main advantage of the evolutionary algorithm is that it can attempt to describe the specific functional form of the data, providing a specific functional expression between the past, present and future values of the time series data. Even if the data is sparse, the evolutionary algorithm is applicable. For a univariate time series, the DEA tries to solve the $P(\cdot)$ defined in formula (8); in addition, the possibility of calculating long-term predictability is discussed. Specifically, for a model:

$$\begin{aligned} x(t) = P'(&x(t-\mu\tau), x(t-(\mu+1)\tau), \\ &\cdots, x(t-(\mu+m-1)\tau)) \end{aligned} \tag{9}$$

Here, the parameter μ determines the long-term predictability. In addition, for a problem requiring μ-step prediction in advance, tests show that the prediction effect of the mapping function $P'(\cdot)$ calculated by formula (9) is much better than that of formula (8) [45]; [48], [49].

2) SPECIFIC STEPS OF THE DARWIN EVOLUTIONARY ALGORITHM

a: GENERATION OF THE INITIAL POPULATION

The original population in the evolutionary process is the population consisting of the original individuals, and this is the basis for generation of new species in the future. If the initial estimate of the potential solution for a problem cannot be obtained, the usual method is to consider a randomly generated population of equations, which is obtained by a random combination of parameters and operators. In this process, the properties, parameters or operators of each element in the string are determined randomly to provide specific values of parameters or operators, and the final individuals must be a consistent mathematical expression. Before introducing the rules for establishing random mathematical consistent strings in suffix representation, we introduce some concepts first. For the convenience of processing, the string of an equation is written as a pair of coordinates. The second coordinate in the coordinate pair represents the parameter or operator in the equation, and we make the following regulations: the coordinate pair (k_1,1) represents the operator in the equation, and the range of k_1 is 1-4, corresponding to addition, subtraction, multiplication and division respectively. The coordinate pair (k_2,2) represents a real parameter. The coordinate pair (k_3, λ) represents a parameter, which can be expressed by time series $x(t\text{-}k_3\tau)$; the range of λ is greater than 11. When we translate coordinate pairs into equation strings, we usually calculate them from left to right, and the two parameters connected by operators are the two closely consecutive parameters on the left of operators. For instance, for a code $P_1(\cdot) = \{(3.2, 2), (3, 11), (1, 1), (5, 11), (3, 1)\}$, we first calculate $\{(3.2, 2), (3, 11), (1, 1)\}$ and the result is $3.2+x(t-3\tau)$. After that, we take the result of the first step as a whole and calculate subsequent results according to the definition of operator in turn; finally, we get $(3.2 + x(t-3\tau))x(t-5\tau)$, which is the final result. The rules for establishing random mathematical consistent strings in suffix representation are as follows: (a) The first two elements of the string must be parameters and the last element must be an operator. (b) Given a position in a string, the number of parameters on the left must be greater than the number of operators. (c) The total number of parameters in the string must be the total number of operators plus 1.

b: COMPUTE POWERFUL INDIVIDUALS

Generally, the strength of the evaluation standard for each individual (equation string) in the population is its fitness. Each individual $P_j(\cdot)$ will be used as a function of the previous values of the time series in order to calculate the estimated values of all $x(t)$ in the time series, which is called the training set. For a prediction problem of advance μ step, the specific fitness calculation formula of $P_j(\cdot)$ is as follows:

$$\Delta_j^2 = \sum_{t-L+1}^{T} (x(t) - P_j(x(t-\mu\tau), x(t-(\mu+1)\tau), \cdots, x(t-(\mu+m-1)\tau)))^2 \tag{10}$$

where P_j represents the *j-th* generation equation string in the population, $L = m\tau$ and T is the total length of the training set. The numerical calculation of each suffix expression P_j uses a stacking method to stack the parameters of the expression until the operator meets the conditions [48]. The intensity index for each individual can be expressed as:

$$R_j = 1 - \frac{\Delta_j^2}{\sum_{t=L+1}^{T} (x(t) - \bar{x})^2} \tag{11}$$

where $\bar{x}$ is the average value of the training data. R_j is the explanatory variance which is a percentage of the total explained variance of the training set in the *j-th* generation equation string. The closer R_j is to 1, the stronger the generation *j* is. The validation or sampling test set is composed of the data not included in the training set, and over fitting will occur when the last individual in the validation set is weak. The final best individual strength index allows for differences in the case of obtaining a good estimate of the dynamic system from the over fitting state.

c: REPLICATION AND VARIATION

Once two parents are chosen according to their power, two new offspring will be produced by crossing the independent parts between the two parents. Only a scheme that can consider cross operation is described here. First, the process determines randomly a parameter, a real number or an element of the time series; if the next element to the right of this randomly selected parameter is an operator, only this parameter is considered for exchange; if the next pair of randomly selected parameters represents another parameter, the string used for cross operation is limited to the case where the number of parameters *nar* and the number of operators *nop* satisfies $nar = nop + 1$. If none of the above conditions are met, another parameter in the string is selected randomly. Note that the goal of this process is to exchange the self-contained parts in equation strings to avoid inconsistent mathematical expressions in the offspring. The same operation is performed on the second equation string. As an example of reproduction, consider the equation string for the parents:

$$\begin{aligned} P_1(\cdot) &= \{(3.2, 2), (3, 11), (1, 1), \overbrace{(5, 11)}^{\text{selected}}, (3, 1)\} \\ &\equiv (3.2 + x(t - 3\tau))x(t - 5\tau) \\ P_2(\cdot) &= \{(1, 11), \underbrace{(2,11)}_{\text{selected}}, (4, 11), (4, 1), (2, 1)\} \\ &\equiv (x(t - \tau) - \frac{x(t - 2\tau)}{x(t - 4\tau)}) \end{aligned} \tag{12}$$

For an example of a scalar time series, a possible pair of offspring is as follows:

$$\begin{aligned} P_3(\cdot) &= \{(3.2, 2), (3,11), (1, 1), (2, 11), (4,11), (4,1), (3, 1)\} \\ &\equiv (3.2 + x(t - 3\tau))(\frac{x(t - 2\tau)}{x(t - 4\tau)}) \\ P_4(\cdot) &= \{(1, 11), (5, 11), (2, 1), \} \\ &\equiv (x(t - \tau) - x(t - 5\tau)), \end{aligned} \tag{13}$$

The bold pair represents the cross part of the parent equation. The substring can be longer than the parent string, but it is always bounded by the maximum length of *ntot*. If the offspring generated by the exchange of the self-contained parts between the parent strings is longer than *ntot*, this specific exchange is not allowed. At this time, another self-contained part in the one parent string will be randomly selected for exchange. This process will be repeated until the conditions are met. Two ectypes of the parent string are also considered offspring during the replication process. Except for the highest ranked equation string, mutations can occur in any individual of the population. Every element of a given string can be changed by a mutation process. In the previous example, the string $P_4(\cdot) = \{(1, 11), (5, 11), (2, 1)\}$ can be changed to $P_4(\cdot) = \{(1, 11), (8.9, 2), (2, 1)\}$, where bold characters represent mutations.

d: THE PARAMETER SETTINGS

In this test, the first 250 data of the time series sample X' are also selected as training samples and the last 115 data are selected as test samples to realize the prediction and analysis of time series X'. There are 13 parameters to be set in the DEA, and the details are as follows:

npop: the number of individuals in the population

ntot: the total number of parameters and operators, that is: $nar + nop$

nsize: the parameters and operators of the initial individual

idum: starting from different initial random populations

nstep: the generations of algorithm termination

ndel: the embedding dimension m (see equation (8))

tau: the time delay element τ, (see equation (8))

nseries: the number of time series to be solved

threshold: μ in the corresponding equation (9)

ndat: the total number of time series

ntdat: the last data point of the training set

pm: the probability of mutation

Rrange: The allowable range of the numeric parameters [-range, range]

Similarly, the parameter selection is also based on grid search method. According to the actual needs and prediction results, the set of final parameters in this paper is shown in table 3 and the flow chart of the experiment is shown in figure 4.

IV. RESULTS AND DISCUSSION

After setting the parameters of the algorithm, the last 115 data of the time series were selected as the test set to verify their prediction effect. Figures 5, 6 and 7 show the trend charts of the predicted results and the real values for the three algorithms respectively.

It can be seen from Figures 5, 6 and 7 that the prediction trends for the three algorithms are both essentially the same as the true value data. However, the prediction results for the

TABLE 3. The specific values parameters of DEA.

Parameter	Specific value
npop	120
ntot	20
nsize	7
idum	123359979
nstep	10000
ndel	3
tau	1
nseries	1
threshold	1
ndat	365
ntdat	250
pm	0.1
Range	10

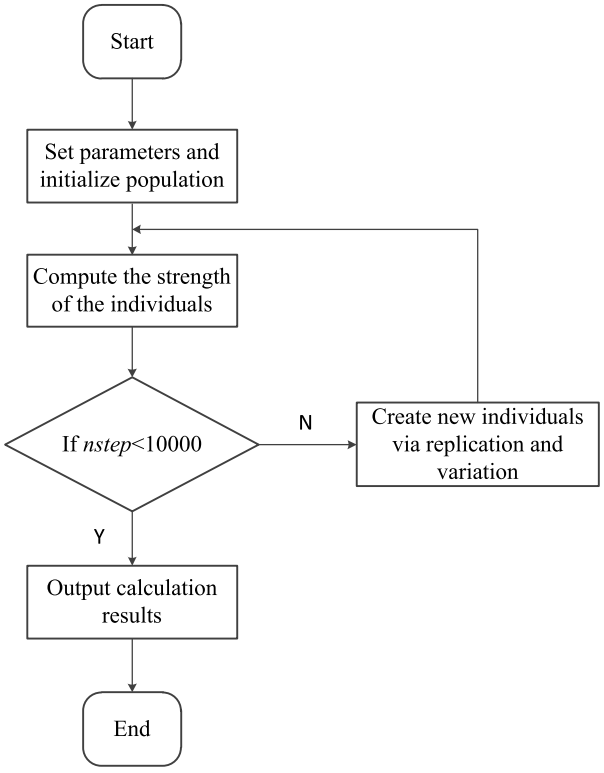

FIGURE 4. The flow chart of the experiment.

DEA are significantly better than that of other algorithms at both ends of the time series in the case of data where there are some fluctuations. To further measure the prediction accuracy, the root mean square error (RMSE) and the mean absolute percent error (MAPE) were used to measure the overall prediction effect of both performance measures. The

TABLE 4. Overall error for the algorithm.

	RMSE (m)	MAPE (%)
SVR	0.2422	2.3286
BP	0.2506	2.5166
DARWIN	0.2248	2.1294

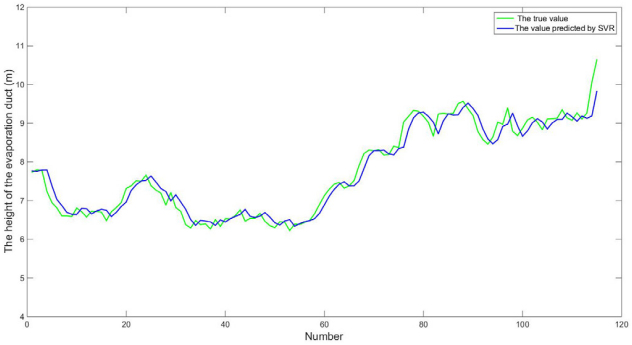

FIGURE 5. The prediction results for the SVR. Abscissa is the sequence of time series, from September 1, 2009 to December 31, 2009, a total of 122 data. The vertical coordinate is the predicted value of EDH on that day.

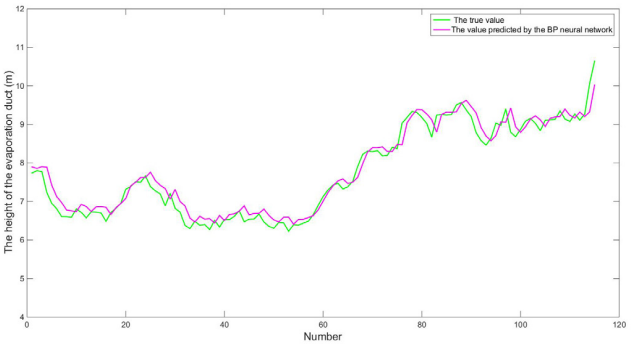

FIGURE 6. The prediction results for the BP neural network. Abscissa is the sequence of time series, from September 1, 2009 to December 31, 2009, a total of 122 data. The vertical coordinate is the predicted value of EDH on that day.

specific formulae used for calculation were as follows:

$$RMSE = \sqrt{\frac{\sum_{i=1}^{N} (X_{obs,i} - X_{\mathrm{mod}\,el,i})^2}{N}} \tag{14}$$

$$MAPE = \frac{1}{N} \sum_{i=1}^{N} \frac{\left| X_{obs,i} - X_{\mathrm{mod}\,el,i} \right|}{X_{obs,i}} \times 100\% \tag{15}$$

Table 4 shows the RMSE and the MAPE of the prediction results for the three algorithms.

From Table 4, it can be seen that the RMSE of the SVR and BP neural network were 0.2422 and 0.2506 respectively, whereas that of the DEA was 0.2248; that is, the RMSE for the DEA was about 7% less than that for the SVR and 10% less than BP neural network. In the case of the MAPE,

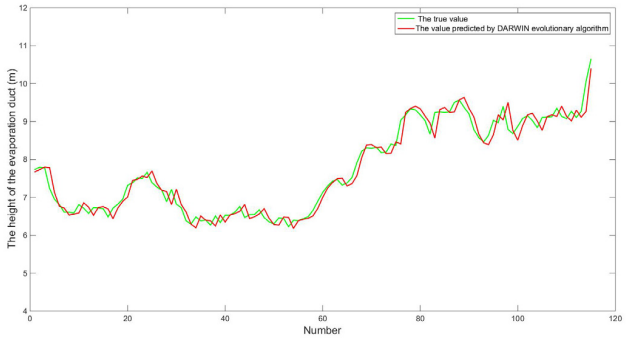

FIGURE 7. The prediction results for the Darwinian evolutionary algorithm. Abscissa is the sequence of time series, from September 1, 2009 to December 31, 2009, a total of 122 data. The vertical coordinate is the predicted value of EDH on that day.

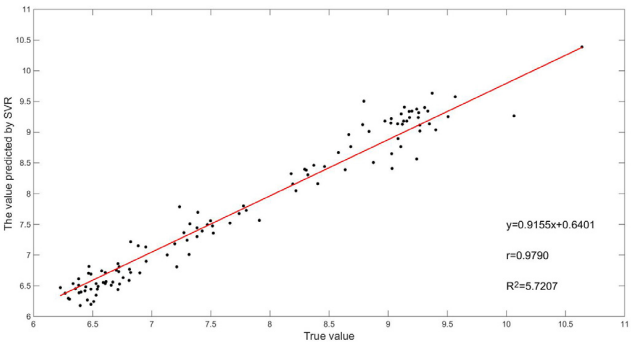

FIGURE 8. Linear regression of the prediction results for the SVR.

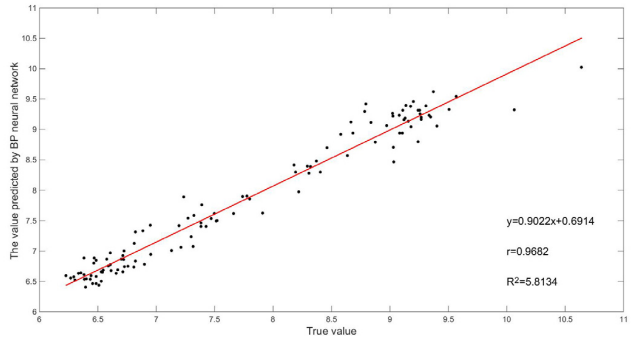

FIGURE 9. Linear regression of the prediction results for the BP neural network.

that of the SVR and BP neural network was 2.3286 and 2.5166 respectively, compared to 2.1294 for the DEA; thus, the value for the DEA was about 9% less than that for the SVR and 15% less than that of BP neural network. These results demonstrated that the overall prediction accuracy of the DEA was better than that of the SVR and BP neural network. To further verify the advantages and disadvantages of the three algorithms, univariate linear regression of the prediction results for the three algorithms was performed, and the regression results are presented in Figures 8, 9 and 10 respectively.

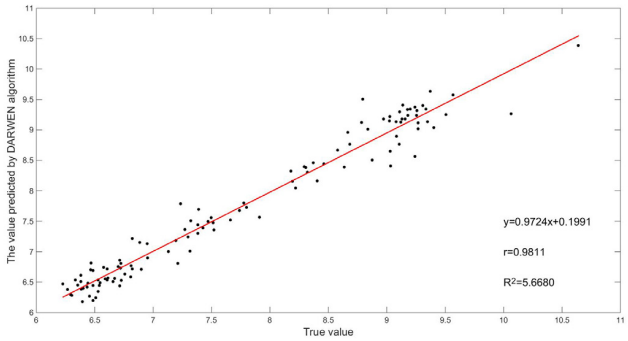

FIGURE 10. Linear regression of the prediction results for the Darwin evolutionary algorithm.

From Figures 8, 9 and 10, it can be seen that the correlation coefficient r for figure 8 (SVR) is 0.9790, the correlation coefficient r for figure 9 (BP neural network) is 0.9682, and the correlation coefficient r for figure 10 is 0.9811 (DEA), confirming that the prediction result for the DEA is slightly better than that of the SVR and BP neural network. Also, the sum of the squared residuals for figure 10 is 5.6680, and that for Figure 8 and 9 is 5.7207 and 5.8134 respectively, indicating that the prediction error for the DEA is smaller than that of the SVR and BP neural network. In addition, the DEA also gave an approximate fitting expression (expression 14) for this time series, and this can be used to describe the development trend of the time series, this being the main advantage of this algorithm.

$$x(t) = (x(t-1) + ((x(t-1) - x(t-3))/((x(t-2) * (x(t-2)/x(t-3))) - ((x(t-1)/(x(t-2)/x(t-1))) + (-4.46))))) \quad (16)$$

V. CONCLUSION

Chaotic time series is the change of some states of chaotic system with time. It has random and nonlinear characteristics. Evaporation duct is an abnormal refraction structure over the ocean; because it is subject to turbulence, weather and other meteorological factors, it is a typical chaotic phenomenon.

In this paper, a new chaos prediction algorithm is introduced, which is applied to obtain the nonlinear formula $P(\cdot)$ of the chaotic phenomenon. Based on the Darwinian natural selection and survival theory, the method first selects appropriate training samples, then produces an initial population before going through an evolutionary process of selection, reproduction and mutation until the optimal individual is found. Finally, a specific expression for a nonlinear chaotic time series is obtained, which in effect can realize the short-term prediction of the EDH.

After that, the DEA, the SVR and the BP neural network are applied for prediction of the EDH over the ocean. The results show that the RMSE for the prediction result for the DEA is 7% less than that of the SVR and 10% less than that of the BP neural network; the MAPE of the DAE was about 9% less than that of the SVR and 15% less than that of

the BP neural network, indicating that the DEA was superior to the two algorithms in terms of predicting the time series for the EDH. In addition, the DEA also gave an approximate fitting expression for the time series, which provided an important reference point for future research on the EDH. In the future voyage, we can use this algorithm to obtain the EDH in advance based on previous data, so that we can master the information of evaporation duct in advance to effectively avoid its influence on our communication system.

However, the time series fitting expression $x(t)$ obtained in this study is ''static'' and does not update with the introduction of new observations. In addition, in actual work, the evaporation ducts are greatly affected by turbulence, prevailing weather conditions and other factors, which may have a great impact on the time course of atmospheric ducts. Therefore, in future work, we will establish a dynamic time series fitting expression based on specific weather scenarios to achieve more accurate predictions of the EDH.

REFERENCES

[1] S. Kang, Y. Zhang, and H. Wang, ''The characteristics and detection of atmospheric duct,'' in *Atmospheric Ducts in the Troposphere*, Z. Wang, Ed., 3rd ed. Beijing, China: Science Press, 2014, pp. 44–68.
[2] X. M. Guo, S. F. Kang, J. Han, Y. S. Zhang, H. G. Wang, and S. B. Zhang, ''Evaporation duct database and statistical analysis for the Chinese sea areas,'' *Chinese. J. Radio. Sci.*, vol. 28, no. 6, pp. 1147–1152, Dec. 2013.
[3] S. M. Babin and G. D. Dockery, ''LKB-based evaporation duct model comparison with buoy data,'' *J. Appl. Meteorol.*, vol. 41, no. 4, pp. 434–446, Apr. 2002.
[4] Z. Sheng and S.-X. Huang, ''Ocean duct inversion using radar clutter and its noise restraining ability,'' *Acta Phys. Sinica*, vol. 58, no. 6, pp. 4328–4334, Jun. 2009.
[5] G. Yu, A. Liu, and Y. Yang, ''Babin Model of evaporation waveguide diagnosis and its sensitivity analysis,'' *J. Astronaut. Metrol.*, vol. 35, pp. 53–56, Apr. 2015.
[6] S. Yang, X. Li, and J. Wu, ''Adaptability research of evaporation duct predication model based on NPS model,'' *J. Elect. Meas.*, vol. 30, pp. 1899–1906, Dec. 2016.
[7] X. He, J. Guo, J. Wu, X. Li, B. Tian, Y. Zhong, and S. Yang, ''Short-term forecast for evaporation duct height based on time series,'' *J. Elect. Meas.*, vol. 32, pp. 102–103, Jan. 2018.
[8] L. Liu, Y. Li, Z. Gao, X. Bi, and G. Zhu, ''Comparison and analysis of four kinds of evaporation duct model,'' *J. Meteorol. Sci.*, vol. 39, pp. 82–96, Feb. 2019.
[9] Y. Shi, Q. Zhang, S. Wang, K. Yang, Y. Yang, X. Yan, and Y. Ma, ''A comprehensive study on maximum wavelength of electromagnetic propagation in different evaporation ducts,'' *IEEE Access*, vol. 7, pp. 82308–82319, 2019.
[10] Y. Mai, Z. Sheng, H. Shi, C. Li, L. Liu, Q. Liao, W. Zhang, and S. Zhou, ''A new diagnostic model and improved prediction algorithm for the heights of evaporation ducts,'' *Frontiers Earth Sci.*, vol. 8, p. 102, Apr. 2020.
[11] L. Liu, Y. Li, Z. Gao, X. Bi, and Q. Chen, ''The prediction model of evaporation duct based on non-iterative sea air flux algorithm,'' *J. Appl. Oceanogr.*, vol. 36, pp. 23–25, Nov. 2017.
[12] Z. Sheng and S.-X. Huang, ''Ocean duct inversion from radar clutter using variation adjoint and regularization method (II): Inversion experiment,'' *Acta Phys. Sinica*, vol. 59, no. 6, pp. 3912–3916, Jun. 2010.
[13] S. Haji Aghajany and Y. Amerian, ''Three dimensional ray tracing technique for tropospheric water vapor tomography using GPS measurements,'' *J. Atmos. Solar-Terr. Phys.*, vol. 164, pp. 81–88, Nov. 2017.
[14] S. Haji-Aghajany and Y. Amerian, ''Hybrid regularized GPS tropospheric sensing using 3-D ray tracing technique,'' *IEEE Geosci. Remote Sens. Lett.*, vol. 15, no. 10, pp. 1475–1479, Oct. 2018.
[15] L. L. Freitas and E. Costa, ''Ray tracing and applications to an evaporation duct model based on data from oceanographic buoy sensors,'' *J. Microw., Optoelectron. Electromagn. Appl.*, vol. 18, no. 1, pp. 96–113, Mar. 2019.
[16] M. A. Ghorbani, R. Khatibi, M. H. Fazelifard, L. Naghipour, and O. Makarynskyy, ''Short-term wind speed predictions with machine learning techniques,'' *Meteorol. Atmos. Phys.*, vol. 128, no. 1, pp. 57–72, Feb. 2016.
[17] S. Park, J. Im, E. Jang, and J. Rhee, ''Drought assessment and monitoring through blending of multi-sensor indices using machine learning approaches for different climate regions,'' *Agricult. Forest Meteorol.*, vol. 216, pp. 157–169, Jan. 2016.
[18] Y. Mai, Z. Sheng, H. Shi, Q. Liao, and W. Zhang, ''Spatiotemporal distribution of atmospheric ducts in alaska and its relationship with the arctic vortex,'' *Int. J. Antennas Propag.*, vol. 2020, Jan. 2020, Art. no. 9673289.
[19] T. Yuan, S. Chen, J. Huang, D. Wu, H. Lu, G. Zhang, X. Ma, Z. Chen, Y. Luo, and X. Ma, ''Influence of dynamic and thermal forcing on the meridional transport of Taklimakan desert dust in spring and summer,'' *J. Climate*, vol. 32, no. 3, pp. 749–767, Feb. 2019.
[20] L. Cornejo-Bueno, C. Casanova-Mateo, J. Sanz-Justo, E. Cerro-Prada, and S. Salcedo-Sanz, ''Efficient prediction of low-visibility events at airports using machine-learning regression,'' *Boundary-Layer Meteorol.*, vol. 165, no. 2, pp. 349–370, Nov. 2017.
[21] A. Just, M. De Carli, A. Shtein, M. Dorman, A. Lyapustin, and I. Kloog, ''Correcting measurement error in satellite aerosol optical depth with machine learning for modeling $PM_{2.5}$ in the northeastern USA,'' *Remote Sens.*, vol. 10, no. 5, p. 803, May 2018.
[22] H. Chen, V. Chandrasekar, R. Cifelli, and P. Xie, ''A machine learning system for precipitation estimation using satellite and ground radar network observations,'' *IEEE Trans. Geosci. Remote Sens.*, vol. 58, no. 2, pp. 982–994, Feb. 2020.
[23] J. Rhee and J. Im, ''Meteorological drought forecasting for ungauged areas based on machine learning: Using long-range climate forecast and remote sensing data,'' *Agricult. Forest Meteorol.*, vols. 237–238, pp. 105–122, May 2017.
[24] M. Hughes, J. Kodros, J. Pierce, M. West, and N. Riemer, ''Machine learning to predict the global distribution of aerosol mixing state metrics,'' *Atmosphere*, vol. 9, no. 1, p. 15, Jan. 2018.
[25] X. Zhu, J. Li, M. Zhu, Z. Jiang, and Y. Li, ''An evaporation duct height prediction method based on deep learning,'' *IEEE Geosci. Remote Sens. Lett.*, vol. 15, no. 9, pp. 1307–1311, Sep. 2018.
[26] C. Yang, ''A comparison of the machine learning algorithm for evaporation duct estimation,'' *Radioengineering*, vol. 22, no. 2, pp. 657–661, Jun. 2013.
[27] Y. He, Z. Sheng, and M. He, ''Spectral analysis of gravity waves from near space high-resolution balloon data in northwest China,'' *Atmosphere*, vol. 11, no. 2, p. 133, Jan. 2020.
[28] X. He, ''Short term forecasting of evaporation duct height based on the time series and neural network,'' M.S. thesis, Tianjin Univ., Tianjin, China, 2017, pp. 21–22.
[29] J. Huang, ''The analysis of time series,'' in *The Meteorological Statistical Analysis and Forecast Method*, R. Zhang, Ed., 3rd ed. Beijing, China: Meteorology, 2004, pp. 199–201.
[30] Y. Zhang, T. Wang, H. Zhao, Y. Zhang, and H. Zhao, ''Multiple radar subbands fusion algorithm based on support vector regression in complex noise environment,'' *IEEE Trans. Antennas Propag.*, vol. 66, no. 1, pp. 381–392, Jan. 2018.
[31] M. Valizadeh and M. R. Sohrabi, ''The application of artificial neural networks and support vector regression for simultaneous spectrophotometric determination of commercial eye drop contents,'' *Spectrochimica Acta A, Mol. Biomol. Spectrosc.*, vol. 193, pp. 297–304, Mar. 2018.
[32] J. D. Martin, Y. T. Morton, and Q. Zhou, ''Neural network development for the forecasting of upper atmosphere parameter distributions,'' *Adv. Space Res.*, vol. 36, no. 12, pp. 2480–2485, 2005.
[33] S. H. Aghajany, B. Voosoghi, and A. Yazdian, ''Estimation of north Tabriz fault parameters using neural networks and 3D tropospherically corrected surface displacement field,'' *Geomatics, Natural Hazards Risk*, vol. 8, no. 2, pp. 918–932, Feb. 2017.
[34] J. Yi, Q. Wang, D. Zhao, and J. T. Wen, ''BP neural network prediction-based variable-period sampling approach for networked control systems,'' *Appl. Math. Comput.*, vol. 185, no. 2, pp. 976–988, Feb. 2007.
[35] Y. Zhao, J. Nan, F.-Y. Cui, and L. Guo, ''Water quality forecast through application of BP neural network at Yuqiao reservoir,'' *J. Zhejiang Univ.-Sci. A*, vol. 8, no. 9, pp. 1482–1487, Aug. 2007.
[36] M. Casdagli, S. Eubank, J. Farmer, D. Desjardins, N. Hunter, and J. Theiler, *Nonlinear Modeling of Chaotic Time Series: Theory and Applications*, Z. Wang, Ed. Hoboken, NJ, USA: Wiley, 1992, pp. 335–381.

[37] A. Saranli and B. Baykal, "Chaotic time-series prediction and the Relocating-LMS (RLMS) algorithm for radial basis function networks," in *Proc. 8th Eur. Signal Process. Conf. (EUSIPCO)*, Trieste, Italy, 1996, pp. 1–4.
[38] S. Kurogi, M. Toidani, R. Shigematsu, and K. Matsuo, "Performance improvement via bagging in probabilistic prediction of chaotic time series using similarity of attractors and LOOCV predictable horizon," *Neural Comput. Appl.*, vol. 29, no. 9, pp. 341–349, Jul. 2017.
[39] F. Takens, "Detecting strange attractors in turbulence," in *Dynamical Systems and Turbulence* (Lecture Notes in Mathematics), vol. 898, D.A. Rand and L.-S. Young, Eds. New York, NY, USA: Springer-Verlag, Jan. 1980, pp. 366–381.
[40] P. Grassberger and I. Procaccia, "Measuring the strangeness of strange attractors," *Phys. D, Nonlinear Phenomena*, vol. 9, nos. 1–2, pp. 189–208, Oct. 1983.
[41] A. Tantet, V. Lucarini, F. Lunkeit, and H. Dijkstra, "Crisis of the chaotic attractor of a climate model: A transfer operator approach," *Nonlinearity*, vol. 31, p. 2221, Apr. 2018.
[42] M. Lei, Z. Wang, and Z. Feng, "A method of embedding dimension estimation based on symplectic geometry," *Phys. Lett. A*, vol. 303, nos. 2–3, pp. 179–189, Oct. 2002.
[43] H. D. I. Abarbanel, R. Brown, J. J. Sidorowich, and L. S. Tsimring, "The analysis of observed chaotic data in physical systems," *Rev. Mod. Phys.*, vol. 65, no. 4, pp. 1331–1392, Oct. 1993.
[44] T. Li, Y. Wang, and X. Zhou, "Bifurcation analysis of a first time-delay chaotic system," *Adv. Difference Equ.*, vol. 2019, no. 1, p. 78, Feb. 2019.
[45] C. López, A. Alvarez, and E. Hernández-García, "Forecasting confined spatiotemporal chaos with genetic algorithms," *Phys. Rev. Lett.*, vol. 85, pp. 2300–2303, Oct. 2000.
[46] F. Z. Xing, E. Cambria, and X. Zou, "Predicting evolving chaotic time series with fuzzy neural networks," in *Proc. Int. Joint Conf. Neural Netw. (IJCNN)*, Anchorage, AK, USA, May 2017, pp. 3176–3183.
[47] S. Hu and M. Huang, "A new forecasting algorithm parameters solving method," in *Proc. Int. Conf. Adv. Sci. Technol.*, Haikou, China, 2016, pp. 296–300.
[48] A. Terki, H. Boubertakh, and N. Mansouri, "Synchronization of chaotic systems using genetic and particle swarms algorithms," in *Proc. 8th Int. Conf. Model., Identificat. Control (ICMIC)*, Algiers, Algeria, Nov. 2016, pp. 671–676.
[49] G. G. Szpiro, "Forecasting chaotic time series with genetic algorithms," *Phys. Rev. E, Stat. Phys. Plasmas Fluids Relat. Interdiscip. Top.*, vol. 55, no. 3, pp. 2557–2568, Mar. 1997.
[50] H. Demirci, A. Özcerit, H. Ekiz, and A. Kutlu, "Chaotic crossover operator on genetic algorithm," *J. Adv. Inform. Technol.*, vol. 6, no. 4, p. 217, Nov. 2015.

YANBO MAI received the B. A. degree from Lanzhou University, Lanzhou, China, in 2018. He is currently pursuing the master's degree with the College of Meteorology and Oceanography, National University of Defense Technology, Changsha, China. His research interests include atmospheric ducts, sensors, and machine learning.

ZHENG SHENG received the B.S., M.S., and Ph.D. degrees in atmospheric science from the College of Meteorology and Oceanography, National University of Defense Technology, Nanjing, China. From 2009 to 2015, he was a Research Assistant with the College of Meteorology and Oceanography, National University of Defense Technology, Changsha, where he is currently an Assistant Professor with the Department of Remote Sensing. His research interests include atmosphere and ocean remote sensing, multi-objective optimization, and various applications using evolutionary algorithms.

HANQING SHI received the B.S., M.S., and Ph.D. degrees in atmospheric science from the College of Meteorology and Oceanography, National University of Defense Technology, Nanjing, China. From 2004 to 2015, he was a Professor with the College of Meteorology and Oceanography, National University of Defense Technology, Changsha, where he is currently a Professor. His research interests include machine learning, deep learning, and optimization methods on atmosphere and ocean satellite remote sensing.

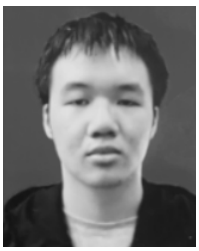

CHAOLEI LI is currently pursuing the degree with Southeast University, Nanjing, China. His research interests include machine learning and parameter optimization.

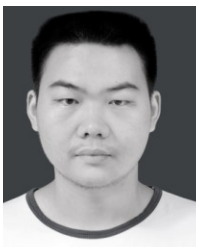

QIXIANG LIAO received the Ph.D. degree from the National University of Defense Technology, Nanjing, China, in 2019. He is currently a Lecturer with the College of Meteorology and Oceanography, National University of Defense Technology, Changsha. His research interests include optimization methods on atmosphere and ocean satellite remote sensing.

JUN BAO received the M.S. degree in physics from the College of Science, National University of Defense Technology, Changsha, China. He is currently a Meteorological Engineer with the China Satellite Maritime Tracking and Control Department. His research interests include optimization methods on atmosphere and ocean satellite remote sensing.